



1 **Measurement Report: Effects of anthropogenic emissions and**
2 **environmental factors on biogenic secondary organic aerosol**
3 **(BSOA) formation in a coastal city of Southeastern China**

4
5 Youwei Hong^{a,b,c,d*}, Xinbei Xu^{a,b,c}, Dan Liao^e, Taotao Liu^{a,b,c}, Xiaoting Ji^{a,b,c}, Ke Xu^{a,b,d},
6 Chunyang Liao^f, Ting Wang^g, Chunshui Lin^g, Jinsheng Chen^{a,b,c*}

7

8 ^aCenter for Excellence in Regional Atmospheric Environment, Institute of Urban Environment,
9 Chinese Academy of Sciences, Xiamen, 361021, China

10 ^bKey Lab of Urban Environment and Health, Institute of Urban Environment, Chinese Academy
11 of Sciences, Xiamen, 361021, China

12 ^cUniversity of Chinese Academy of Sciences, Beijing, 100049, China

13 ^dSchool of Life Sciences, Hebei University, Baoding, 071000, China

14 ^eCollege of Environment and Public Health, Xiamen Huaxia University, Xiamen 361024, China

15 ^fState Key Laboratory of Environmental Chemistry and Ecotoxicology, Research Center for Eco-
16 Environmental Sciences, Chinese Academy of Sciences, Beijing 100085, China

17 ^g Institute of Earth Environment, Chinese Academy of Sciences, Xi'an, 710061, China

18

19 *Corresponding author E-mail: Jinsheng Chen (jschen@iue.ac.cn); Youwei Hong
20 (ywhong@iue.ac.cn)

21

22

23

24

25

26

27

28

29

30

31

32

33



34 **Abstract:**

35 To better understand the formation of biogenic secondary organic aerosol (BSOA),
36 aerosol samples with a 4 h time resolution were collected during summer and
37 wintertime in the southeast of China, along with on-line measurements of trace gases,
38 aerosol chemical compositions, and meteorological parameters. The samples were
39 analyzed by gas chromatography-mass spectrometry for PM_{2.5}-bound SOA tracers,
40 including isoprene (SOA_I), α/β -pinene (SOA_M), β -caryophyllene (SOA_C), and toluene
41 (ASOA). The average concentrations of total SOA tracers in winter and summer were
42 38.8 and 111.9 ng m⁻³, respectively, with the predominance of SOA_M (70.1% and
43 45.8%), followed by SOA_I (14.0% and 45.6%), ASOA (11.0% and 6.2%) and SOA_C
44 (4.9% and 2.3%). Compare to those in winter, the majority of BSOA tracers in summer
45 showed significant positive correlations with Ox (O₃+NO₂), HONO, ultraviolet (UV)
46 and temperature (T), indicating the influence of photochemical oxidation under
47 relatively clean conditions. However, in winter, BSOA tracers were significantly
48 correlated with PM_{2.5}, NO₃⁻, SO₄²⁻, and NH₃, attributed to the contributions of
49 anthropogenic emissions. Major BSOA tracers in both seasons was linearly correlated
50 with aerosol acidity (pH), liquid water content (LWC) and SO₄²⁻. The results indicated
51 that acid-catalyzed reactive uptake onto sulfate aerosol particles enhanced the
52 formation of BSOA. In summer, the clean air mass originated from the ocean, and
53 chlorine depletion was observed. We also found that concentrations of the total SOA
54 tracers was correlated with HCl and chlorine ions in PM_{2.5}, reflecting the contribution
55 of Cl-initiated VOC oxidations to the formation of SOA. In winter, the northeast
56 dominant wind direction brought continental polluted air mass to the monitoring site,
57 affecting the transformation of BSOA tracers. This implied that anthropogenic
58 emissions, atmospheric oxidation capacity and halogen chemistry have significant
59 effects on the formation of BSOA in the southeast coastal area.

60 **Keywords:** SOA tracers; biogenic volatile organic compounds; anthropogenic
61 pollutants; atmospheric oxidation capacity; coastal area

62



63 1. Introduction

64 Secondary organic aerosol (SOA) has attracted widespread scientific researchers
65 concerns, due to its potential impacts on climate change, human health and air quality
66 (Shrivastava et al., 2017; Reid et al., 2018; Zhu et al., 2019; Wang et al., 2021b).
67 Understanding the formation of SOA and assessing its relevance for environmental
68 effects become an integral part of aerosol chemistry (Charan et al., 2019; Xiao et al.,
69 2020; Palmer et al., 2022). However, due to its complex precursors and atmospheric
70 physical or chemical processes, SOA prediction by air quality models remains highly
71 uncertain (McFiggans et al., 2019). Therefore, it is necessary to better explore missed
72 SOA sources and unknown SOA formation mechanisms.

73 SOA was produced by the conversion of biogenic and anthropogenic volatile
74 organic compounds (BVOCs and AVOCs) through complex homogeneous and
75 heterogeneous reactions (Charan et al., 2019; Xiao et al., 2020; Mahilang et al., 2021).
76 BVOCs are the main precursors of SOA on a global scale, while AVOCs are the
77 predominant contributor to SOA in urban areas (Hallquist et al., 2009; Wang et al.,
78 2021a). Recently, laboratory, field observation and model studies have shown that
79 anthropogenic emissions greatly affect the formation of BSOA (Hoyle et al., 2011;
80 Shrivastava et al., 2019; Zhang et al., 2019b; Zhang et al., 2019c; Mahilang et al., 2021;
81 Xu et al., 2021). Anthropogenic air pollutants, such as NO_x, SO₂, NH₃ and aerosols,
82 could influence the conversion of BVOCs to the particulate phase and the production
83 of nitrogen and sulfur compounds (Wang et al., 2020). NO_x is one of the important
84 drivers of SOA formation and yields during both daytime and nighttime through
85 alternating the fate of peroxy radicals (RO₂·) (Sarrafzadeh et al., 2016; Newland et al.,
86 2021). While ·OH dominates the photochemical oxidation of BVOC during daylight
87 hours, and NO₃· becomes one of the main oxidants for biogenic SOA and organic
88 nitrates at night. SO₂ also plays an important role in changing SOA formation from
89 BVOC photooxidation and ozonolysis through sulfuric acid formation and acid-
90 catalyzed heterogeneous reactions (Zhao et al., 2018; Zhang et al., 2019b; Xu et al.,



91 2021). In addition, NH_3 and amines can affect the SOA yields and composition through
92 both gas-phase and heterogeneous reactions, by reacting with sulfuric or nitric acid to
93 generate secondary inorganic aerosols (SIA) (Ma et al., 2018; Liu et al., 2021; Lv et
94 al., 2022). However, due to complex precursors and atmospheric processes, the
95 combined effects of anthropogenic emissions and meteorological factors on the
96 formation of SOA are not fully understood.

97 The coastal area of southeastern China is under the East Asian monsoon control,
98 which cause an obvious alternation of polluted and clean air masses from continental
99 and ocean area, respectively (Wu et al., 2019; Hong et al., 2021). Also, the local
100 geographical environment, including relatively high humidity, dense vegetation and
101 strong atmospheric oxidation capacity, provides a good chance to study the sources and
102 formation mechanisms of SOA. In our previous studies, ground-based observations in
103 a mountainous forest area of this region showed that BSOA tracers were the largest
104 contributor to SOA, and the aerosols were highly oxidized (Hong et al., 2019). However,
105 with the development of rapid urbanization, anthropogenic emissions will be of great
106 significance on SOA formation (Liu et al., 2020). Halogen radicals (chlorine, bromine,
107 iodine) have an important role in tropospheric oxidants chemistry and OA formation
108 (Wang et al., 2021c). Therefore, it is necessary to investigate the sources and formation
109 mechanisms of SOA in coastal urban areas, and so as to provide a scientific basis for
110 the estimation of regional SOA budgets and $\text{PM}_{2.5}$ pollution control.

111 In this study, a continuous $\text{PM}_{2.5}$ sampling campaign with a 4 h time resolution
112 was conducted in a coastal city of southeastern China during the winter and
113 summertime period. Seasonal, diurnal variations and SOC contributions of SOA tracers
114 were analyzed. We also demonstrated the indications of SOA tracers for air pollution
115 process. Finally, the combined effects of anthropogenic emissions and major
116 environmental factors on promoting SOA formation was discussed.

117 **2. Materials and methods**

118 *2.1 Sample collection*



119 The sampling was performed at the Institute of Urban Environment, Chinese
120 Academy of Sciences (118.06° E, 24.61° N), which is located in a suburban area of
121 Xiamen, a coastal city of southeastern China. Detailed information of the air monitoring
122 supersite was described in our previous study (Hong et al., 2021). Briefly, time-resolved
123 (00:00–08:00, 08:00–12:00, 12:00–16:00, 16:00–20:00, 20:00–24:00 CST – China
124 Standard Time) PM_{2.5} samples were collected on the rooftop of the station (about 70m
125 above the ground). The sampling was carried out by using a high volume (1.05 m³ min⁻¹)
126 sampler (TH-1000C, Wuhan Tianhong, China) with a PM_{2.5} inlet from 10 to 18 January,
127 and from 5 to 14 July 2020. All samples were collected onto pre-baked (450 °C, 6 h)
128 quartz fiber filters. Field blank samples were also collected. The sample filters were
129 separately sealed in aluminum foil and stored in a freezer (–20 °C) prior to analysis.

130 2.2 SOA tracers analysis by GC/MS

131 The isoprene-derived SOA (SOA_I) tracers included 2 methyltetrols (MTLs: 2-
132 methylthreitol (MTL1) and 2-methylerythritol (MTL2)), C5-alkene triols (cis-2-
133 methyl-1,3,4-trihydroxy-1-butene, trans-2-methyl-1,3,4-trihydroxy-1-butene, and 3-
134 methyl-2,3,4-trihydroxy-1-butene) and 2-methylglyceric acid (MGA). The
135 monoterpene-derived SOA (SOA_M) tracers were composed of pinic acid (PA), pinonic
136 acid (PNA), 3-hydroxyglutaric acid (HGA), 3-methyl-1,2,3-butanetricarboxylic acid
137 (MBTCA), 3-hydro-4,4-dimethylglutaric acid (HDMGA), and 3-acetylglutaric acid
138 (AGA). The β-caryophyllene-derived SOA (SOA_C) tracer was β-caryophyllenic acid
139 (CA), the toluene-derived SOA (SOA_A) tracer was 2,3-Dihydroxy-4-oxopentanoic acid
140 (DHOPA) and levoglucosan (LEV) as a tracer of biomass burning. Due to the lack of
141 authentic standards, surrogate standards (including erythritol, malic acid, PA and
142 citramalic acid) were used to quantify SOA_I, SOA_M, SOA_C and SOA_A tracer,
143 respectively (Fu et al., 2009). Details of SOA tracer's calculated concentrations based
144 on relative response factors (RRFs) were presented in our previous studies (Hong et al.,
145 2019; Liu et al., 2020).

146 The analytical procedure of fifteen SOA tracers was published in our previous
147 studies (Hong et al., 2019; Liu et al., 2020). Briefly, the filter samples were



148 ultrasonically extracted with a mixture of dichloromethane and methanol (2:1, v/v) for
149 10 min. The extracts were filtered with a PTFE filter (0.22 μm), and dried with high
150 purity N_2 (99.99%), and then derivatized with 60 μL of N,O-bis-(trimethylsilyl)
151 trifluoroacetamide (BSTFA) with 1% trimethylsilyl chloride and 10 μL of pyridine at
152 70 $^\circ\text{C}$ for 3 h. At last, 140 μL of internal standard solution (^{13}C n-alkane solution, 1.507
153 $\text{ng } \mu\text{L}^{-1}$) was added into the samples.

154 Fifteen SOA tracers were determined by GC-MSD (7890A/5975C, Agilent
155 Technologies, Inc., USA) with a DB-5 MS silica capillary column (i.d. 30 \times 0.25 mm,
156 0.25 μm film thickness). 1 μL sample was injected with splitless mode and high purity
157 helium (99.999%) was used as carrier gas at a stable flow of 1.0 mL/min. The GC
158 temperature was initiated at 100 $^\circ\text{C}$ (held for 1 min) and then to 300 $^\circ\text{C}$ at 5 $^\circ\text{C min}^{-1}$,
159 and kept at 300 $^\circ\text{C}$ for 10 min. The operation mode is electron ionization (EI) mode of
160 70 eV. The method detection limits (MDLs) for erythritol and PNA were 0.01 and 0.02
161 ng m^{-3} , respectively. The recoveries of erythritol, PNA, malic acid, PA and citramalic
162 acid were 67 \pm 2%, 73 \pm 1%, 75 \pm 1%, 88 \pm 7% and 82 \pm 8%, respectively. SOA tracers were
163 not detected in the field blank samples.

164 2.3 Observations in the air monitoring supersite

165 Water-soluble inorganic ions (WSII) in $\text{PM}_{2.5}$ (Cl^- , SO_4^{2-} , NO_3^- , Na^+ , K^+ , NH_4^+ ,
166 Mg^{2+} , and Ca^{2+}) and gas pollutants (HCl, HONO, HNO_3 , NH_3) were hourly measured
167 using a monitoring device for aerosols and gases in ambient Air (MARGA 2080;
168 Metrohm Applikon B.V.; Delft, Netherlands). Internal calibration was carried out using
169 LiBr standard solutions. The detection limit of Cl^- , SO_4^{2-} , NO_3^- , Na^+ , K^+ , NH_4^+ , Mg^{2+} ,
170 and Ca^{2+} were 0.01, 0.04, 0.05, 0.05, 0.09, 0.05, 0.06 and 0.09 $\mu\text{g m}^{-3}$, respectively.

171 Hourly mass concentrations of $\text{PM}_{2.5}$ and PM_{10} were measured by using a tapered
172 element oscillating microbalance (TEOM1405, Thermo Scientific Corp., MA, USA).
173 NO_2 , SO_2 , and O_3 were monitored using continuous gas analyzers (TEI 42i, 43i, and
174 49i, Thermo Scientific Corp., MA, USA). Ambient meteorological parameters
175 including relative humidity (RH), temperature (T), wind speed (WS), and wind
176 direction (WD) were obtained by an ultrasonic anemometer (150WX, Airmar, the



177 USA). Photolysis frequencies were determined using a photolysis spectrometer (PFS-
178 100, Focused Photonics Inc., Hangzhou, China), including the photolysis rate constants
179 $J(\text{O}^1\text{D})$, $J(\text{HCHO_M})$, $J(\text{HCHO_R})$, $J(\text{NO}_2)$, $J(\text{H}_2\text{O}_2)$, $J(\text{HONO})$, $J(\text{NO}_3_M)$ and
180 $J(\text{NO}_3_R)$, and the spectral band ranged from 270 to 790 nm. Boundary layer height
181 (BLH) based on ERA-5 reanalysis dataset was downloaded from the following link
182 <https://www.ecmwf.int/en/forecasts/datasets/reanalysis-datasets/era5>.

183 *2.4 Estimation of SOC using a tracer-based method*

184 The fraction of SOC formed by the oxidation of monoterpene, isoprene, β -
185 caryophyllene and toluene was estimated using a tracer-based method (Kleindienst et
186 al., 2007; Hong et al., 2019). It is defined as $[\text{SOC}] = \sum i[\text{tri}]/f_{\text{SOC}}$, where $[\text{SOC}]$
187 represents the mass concentration of SOC ($\mu\text{gC m}^{-3}$) and $\sum i[\text{tri}]$ means the sum of the
188 concentration of individual SOA tracer ($\mu\text{g m}^{-3}$). The carbon mass fractions (f_{SOC}) of
189 monoterpene, isoprene, β -caryophyllene and toluene were 0.231 ± 0.111 , 0.155 ± 0.111 ,
190 0.023 ± 0.005 and 0.008 ± 0.003 , respectively, based on smog-chamber experimental
191 data (Kleindienst et al., 2007).

192 *2.5 Aerosol acidity and OH calculation*

193 The E-AIM IV (Extended Aerosol Inorganic Model IV version) was used to
194 simulate the aqueous and solid phases of ionic compositions in the mixing system (H^+ -
195 NH_4^+ - SO_4^{2-} - NO_3^- - Cl^- - Na^+ - H_2O) at a given T and RH (Friese and Ebel, 2010).
196 According to our previous study (Wu et al., 2020), the hourly averaged T, RH, SO_4^{2-} ,
197 NO_3^- , Cl^- , NH_4^+ , Na^+ and molar concentrations of total aerosol acidity ($\text{H}^+_{\text{total}}$) were
198 used as the input in the model E-AIMIV to obtain the concentrations of free ions
199 (including free H^+ ($\text{H}^+_{\text{insitu}}$) in the aqueous phase, and liquid water content (LWC)).
200 $\text{H}^+_{\text{insitu}}$ defined as the moles of free hydrogen ions in the aqueous phase of aerosols per
201 unit of air ($\text{nmol}\cdot\text{m}^{-3}$), is the actual acidity in the droplets of the aerosols. The $\text{H}^+_{\text{total}}$
202 was estimated from the ionic balance of the relevant ionic species: $\text{H}^+_{\text{total}} =$
203 $2\text{SO}_4^{2-} + \text{NO}_3^- + \text{Cl}^- - \text{NH}_4^+ - \text{Na}^+$.

204 The pH of aerosol was calculated as the follow:



$$\text{pH} = -\lg\left(\frac{\gamma \times \text{H}_{\text{insitu}}^+}{V_{\text{aq}}/1000}\right)$$

205

206 where γ and V_{aq} denote the activity coefficient and the volume of particle aqueous
207 phase in air ($\text{cm}^3\cdot\text{m}$).

208 The forward mode of ISORROPIA II thermodynamic model was run by assuming
209 that aerosol solutions were metastable (only a liquid phase). The pH value from
210 ISORROPIA II was calculated using the following equation:

$$\text{pH} = -\lg\left(\frac{1000 \times \text{H}^+}{\text{LWC}}\right)$$

211

212 where H^+ is the equilibrium particle hydronium ion concentration per volume air.

213 The OH concentration ([OH]) was estimated using the NO_2 and HONO
214 concentrations and the photolysis rate constants (J) of NO_2 , O_3 , and HONO, according
215 to the following improved empirical formula (Wen et al., 2019).

$$216 \quad [\text{OH}] = 4.1 \times 10^9 \times \frac{J(\text{O}^1\text{D})^{0.83} \times J(\text{NO}_2)^{0.19} \times (140 \times \text{NO}_2 + 1) + \text{HONO} \times J(\text{HONO})}{0.41 \times \text{NO}_2^2 + 1.7 \times \text{NO}_2 + 1 + \text{NO} \times k_{\text{NO}+\text{OH}} + \text{HONO} \times k_{\text{HONO}+\text{OH}}}$$

217 2.6 Statistical analysis

218 Correlation analysis by SPSS 22.0 software (IBM, Armonk, NY, USA) was used
219 to study the relationship among SOA tracers, meteorological parameters and criteria air
220 pollutants. One-way analysis of variance (ANOVA) was adopted to examine the
221 variations of different factors.

222 2.7. Backward trajectory analysis

223 Hybrid Single-Particle Lagrangian Integrated Trajectory (HYSPLIT) was used to
224 analyze the impacts of air masses on Xiamen during different seasons. 72 h backward
225 trajectories were calculated every hour at a height of 500 m. The meteorological data
226 with a resolution of 1° longitude \times 1° latitude was obtained from the NCEP/GDAS.
227 Cluster analysis was adopted using the total spatial variance (TSV).

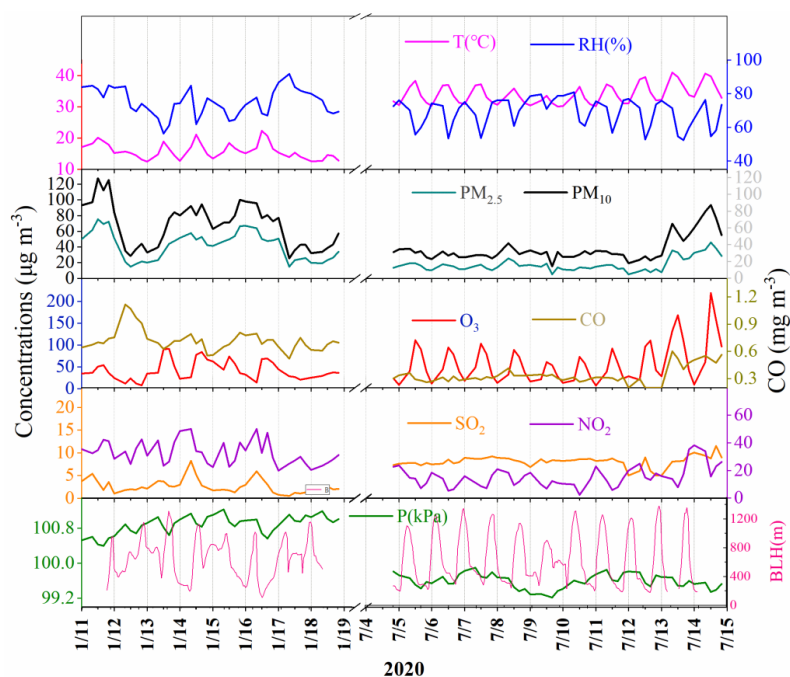
228 3 Results and discussion

229 3.1. Overview of air pollutants

230 The concentrations of criteria air pollutants, including SO_2 , CO, NO_2 , O_3 , $\text{PM}_{2.5}$



231 and PM₁₀, and meteorological parameters during wintertime and summertime were
232 shown in Fig.1. The concentrations of PM_{2.5} in winter ranged from 14.9 to 75.3 $\mu\text{g m}^{-3}$
233 with an average of 42.1 $\mu\text{g m}^{-3}$, which was much higher than that (the average of 18.4
234 $\mu\text{g m}^{-3}$) in summer, ranging from 12.8 to 46.4 $\mu\text{g m}^{-3}$. The concentrations of CO, NO₂
235 and PM₁₀ showed similar seasonal trends to the pattern of PM_{2.5}. In contrast, O₃ had the
236 highest concentration in summer, which was attributed to the formation of
237 photochemical reaction under strong UV radiation and the weak titration of nitrogen
238 oxides. Meanwhile, the concentrations of SO₂ ($8.37\pm 0.79 \mu\text{g m}^{-3}$) in summer was also
239 higher than that ($2.63\pm 1.95 \mu\text{g m}^{-3}$) in winter, mainly attributed to the influence of coal
240 combustion and ship emissions. The monitoring site was located approximately 15 km
241 away from Xiamen port area and a coal-fired power plant ($4 \times 300 \text{ kW}$) in the south.
242 Southerly winds were prevailed in summer, which might cause the relative high
243 concentration of SO₂ in the monitoring site.



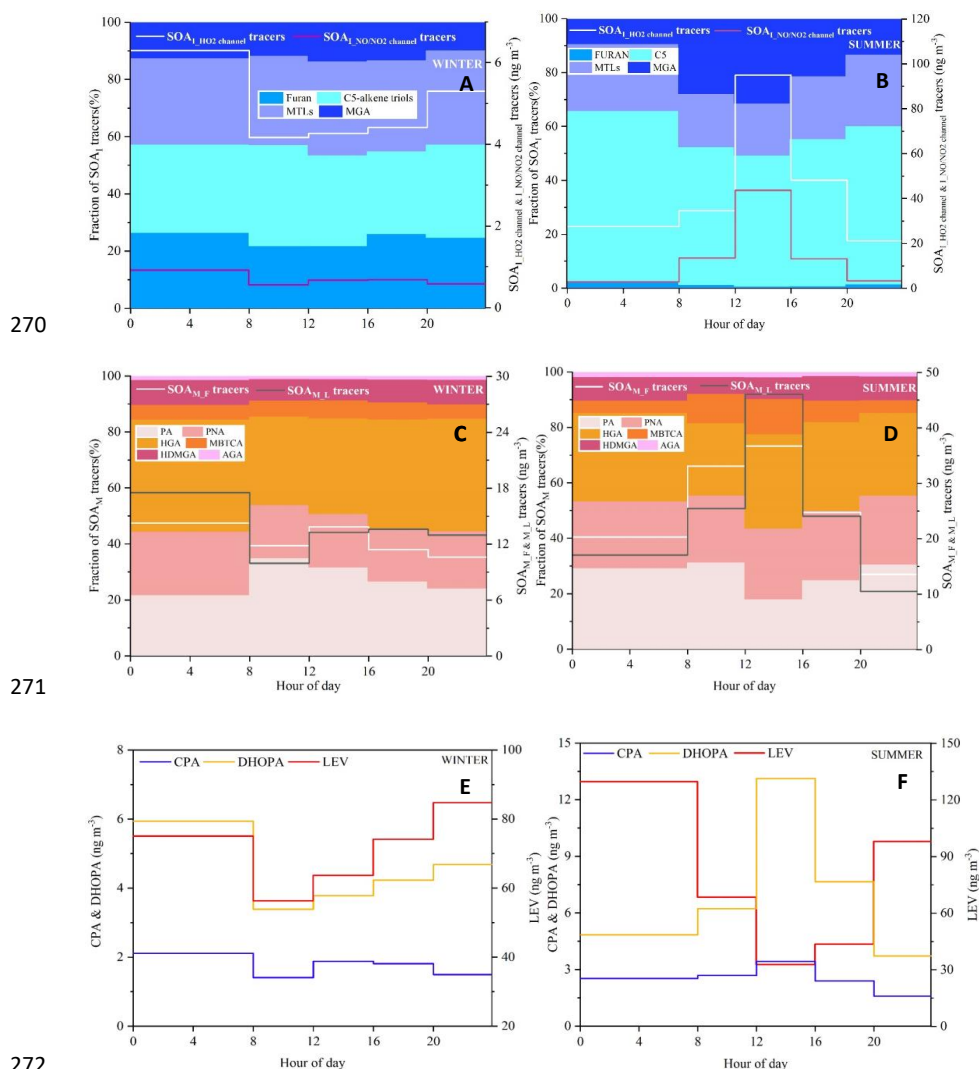
244

245 **Figure 1. Time series of criteria air pollutants and meteorological parameters**
246 **during the sampling period**



247 *3.2 Temporal variations of SOA tracers and estimated SOC*

248 Temporal variations of individual SOA tracer are shown in Fig.S1. The average
249 concentrations of total SOA tracers in winter and summer were 38.8 and 111.9 ng m^{-3} ,
250 respectively, with the predominance of SOA_M , followed by SOA_I and SOA_C . In
251 summer, BSOA tracers showed much higher concentrations in the daytime than in the
252 nighttime, while inverse results were observed in winter. For example, in summer,
253 SOA_I in the daytime ranged from 21.3 to 293.2 ng m^{-3} (average of $82.6 \pm 65.3 \text{ ng m}^{-3}$)
254 and the concentrations of SOA_I ranging from 6.81 to 110.1 ng m^{-3} (average of
255 $27.4 \pm 24.6 \text{ ng m}^{-3}$) were observed in the nighttime. However, in winter, the
256 concentrations of isoprene SOA tracers in the daytime ranging from 1.36 to 11.1 ng m^{-3}
257 (average of $4.93 \pm 2.62 \text{ ng m}^{-3}$) were lower than those (average of $15.3 \pm 8.32 \text{ ng m}^{-3}$) in
258 the nighttime. As shown in Fig. 2, diurnal variations of SOA_M , SOA_I , CPA and DHOPA
259 tracers in summer showed high levels in the afternoon (12:00–16:00 CST), due to the
260 impacts of beneficial photochemical oxidation conditions caused by high temperature
261 and strong UV radiation. The related SOA tracers were consisted with the emissions of
262 their precursors including biogenic and anthropogenic VOCs, similar to our previous
263 studies (Hong et al., 2019; Liu et al., 2020). However, the SOA tracers in winter showed
264 the lowest concentrations in the morning (8:00–12:00 CST), related with the favorable
265 dispersion conditions caused by the increasing planetary boundary layer height (BLH)
266 (Fig.1). Totally, high concentrations of BSOA tracers was found in the daytime and in
267 summer, indicating the effects of temperature on biogenic VOCs emissions and their
268 photochemical oxidations. And the concentrations of BSOA tracers in winter increased
269 in the nighttime, due to the changing of nocturnal boundary layer.



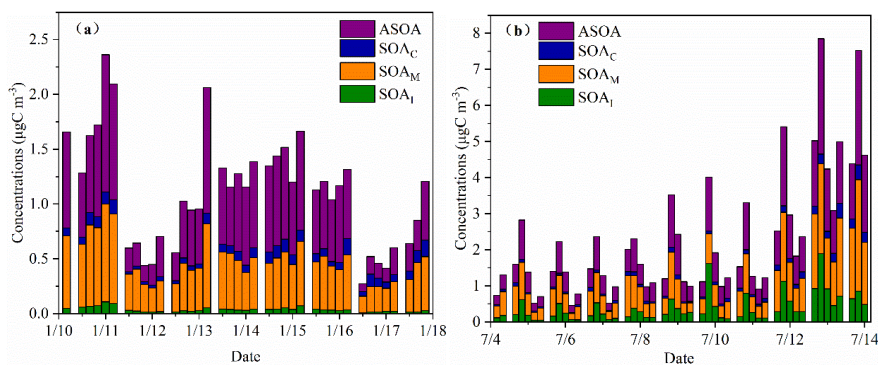
270
 271
 272
 273 **Figure 2. Diurnal variation of individual SOA tracer during the wintertime and**
 274 **summertime**

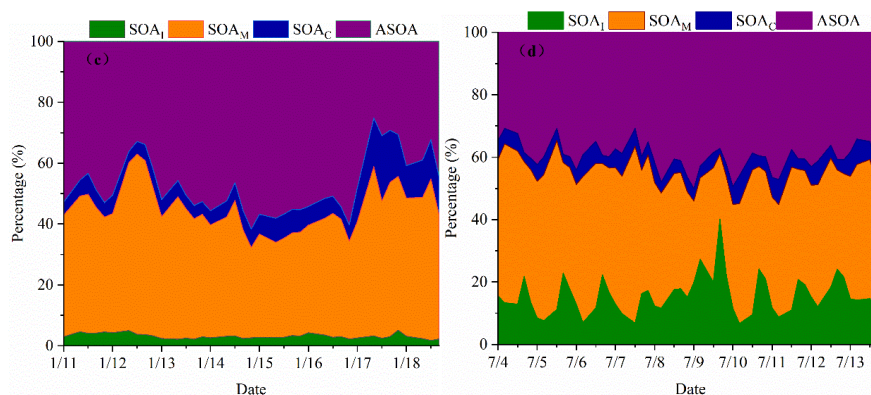
275 As shown in Fig.3a, b, SOA tracers-based SOC in winter and summer was
 276 estimated. The concentrations of SOC in winter ranged from 0.27 to 2.36 $\mu\text{g C m}^{-3}$, with
 277 an average of 1.11 $\mu\text{g C m}^{-3}$. Meanwhile, the concentrations of SOC in summer ranged
 278 from 0.46 to 7.85 $\mu\text{g C m}^{-3}$, with an average of 2.27 $\mu\text{g C m}^{-3}$. The results showed that
 279 the contributions of SOA tracers to SOC in summer was higher than those in winter.



280 For individual SOA tracer, the concentrations of monoterpene-derived SOC ($0.87 \pm$
281 $0.64 \mu\text{g C m}^{-3}$) was comparable to the toluene-derived SOC ($0.90 \pm 0.69 \mu\text{g C m}^{-3}$),
282 which were higher than isoprene-derived SOC ($0.39 \pm 0.38 \mu\text{g C m}^{-3}$) and β -
283 caryophyllene-derived SOC ($0.10 \pm 0.08 \mu\text{g C m}^{-3}$). An obvious trend of diurnal
284 variations of isoprene-derived SOC was observed, which was consistent with a certain
285 amount of isoprene emitted from various plants. However, no similar trend was found
286 in winter. In addition, the toluene, monoterpene, isoprene and β -caryophyllene-derived
287 SOC in summer accounted for 40.0%, 39.2%, 15.7% and 5.1% of the total SOC,
288 respectively (Fig.3c, d). However, in winter, the percentages of toluene, monoterpene,
289 isoprene and β -caryophyllene-derived SOC were 47.2%, 42.1%, 3.2% and 7.6%,
290 respectively. The percentages of isoprene-derived SOC estimated from different
291 precursors varied significantly among the seasons. High temperature enhanced the
292 emissions of isoprene, and strong solar radiation favored the formation of isoprene SOA
293 tracers, contributing to the highest isoprene-derived SOC percentage in summer (Ding
294 et al., 2014). And the highest percentages of toluene-derived SOC (47.2%) in winter
295 were related with anthropogenic emissions and adverse diffusion conditions.

296



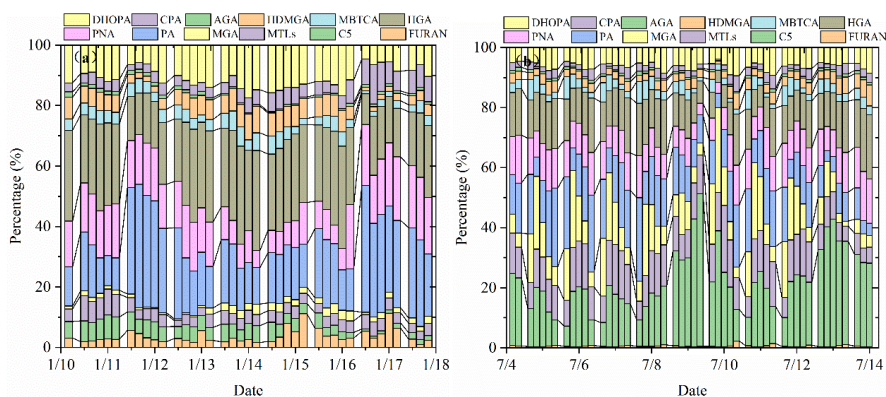


297

298 **Figure 3. Concentrations and percentages of SOA tracer-based estimated SOC**
299 **during the sampling period**

300 3.3 Atmospheric process indication of BSOA tracers

301 As shown in Fig.4, percentages of different types of SOA tracers in winter and
302 summer were calculated. In summer, the monoterpene, isoprene, toluene and β -
303 caryophyllene SOA tracers accounted for 45.8%, 45.6%, 6.2% and 2.3% of the total
304 SOA tracers, respectively. However, in winter, the percentages of monoterpene,
305 isoprene, toluene and β -caryophyllene SOA tracers were 70.1%, 14.0%, 11.0% and
306 4.9%, respectively. The percentage of SOA_I decreased sharply, due to the impacts of
307 temperature on isoprene emissions, which was consisted with our previous findings
308 (Hong et al., 2019). Meanwhile, the concentrations of SOA_M were the largest in both
309 seasons, due to a large amount of monoterpene emissions from the related plant species.
310 Xiamen, an international garden city, located in coastal area of southeastern China.
311 Monoterpene, such as α/β -pinene, is mostly emitted by coniferous plant and most
312 flowers and fruits, while isoprene originates from broad-leaved trees and deciduous
313 plants (Ding et al., 2014; Shrivastava et al., 2017; Yang et al., 2021).



314

315 **Figure 4. Percentages of isoprene, monoterpene, β -caryophyllene and toluene**
316 **SOA tracers in winter (a) and summer (b)**

317 The α/β -pinene SOA tracers, including first generation products (PA, PNA) and
318 later-generation products (HGA, AGA, HDMGA and MBTCA), could be used to
319 evaluate the aging degree of BSOA (Ding et al., 2014; Hong et al., 2019). In this study,
320 HGA (32.2%) was the major component of α/β -pinene tracers, followed by PA (30.5%),
321 PNA (21.8%), HDMGA (7.3%), MBTCA (6.8%), and AGA (1.5%). The percentage of
322 PA and PNA were much higher than those in mountainous background areas (PA: 9%
323 and PNA: 3%)(Hong et al., 2019), suggesting the contribution of preliminary products
324 to SOA in urban areas. As shown in Fig.4, the percentages of PA and PNA in winter
325 (21.8% and 14.2%) were higher than those in summer (14.2% and 10.7%). Reacted
326 with atmospheric oxidants including O_3 and OH, PA and PNA were transformed into
327 MBTCA (Offenberg et al., 2007). This is the reason why the proportions of PA and
328 PNA had a significant decreasing trend from winter to summer. The ratio of
329 MBTCA/(PA+PNA) in summer and winter were 0.16 ± 0.09 and 0.12 ± 0.07 , respectively,
330 which also proved the impacts of atmospheric oxidation capacity on the aging degree
331 of SOA_M . In addition, the ratio of HGA/MBTCA could be used to distinguish the
332 contribution of α -pinene or β -pinene to the SOA_M formation (Jaoui et al., 2005; Ding et
333 al., 2014). The ratio of HGA/MBTCA with an average of 5.78 in Xiamen was high,
334 suggesting the contribution of β -pinene to SOA_M . Low ratio of HGA/MBTCA (~ 1.0)



335 showed that α -pinene was the major precursor for SOA_M (Lewandowski et al., 2013).

336 As shown in Fig.4, MTLs and C5 alkene triols were the main components of the
337 total SOA_I, with an average percentage of $68.0 \pm 14.9\%$, indicating a low-NO_x
338 environment (Ding et al., 2014; Liu et al., 2020). In summer, the percentages of MTLs
339 and C5 alkene triols to the total SOA tracers in summer (21.8% and 14.2%) were
340 obviously higher than those in winter (4.2% and 4.3%). This was consisted with the
341 fact that the concentrations of NO₂ ($14.8 \pm 7.46 \mu\text{g m}^{-3}$) in summer was significantly
342 lower than that ($32.7 \pm 32.6 \mu\text{g m}^{-3}$) in winter. Previous studies found that MTLs and C5
343 alkene triols were formed by the OH and HO₂ radicals via the HO₂ channel under low-
344 NO_x conditions (Surratt et al., 2010). C5 alkene triols are mainly produced by acid
345 catalyzed reaction of Isoprene Epoxydiols (IEPOX) in the gas phase, while MTLs are
346 formed by ring opening products of IEPOX (Surratt et al., 2007; Surratt et al., 2010).
347 And the ozonolysis of isoprene was also an important pathway for MTLs in the
348 presence of acid sulfate aerosols (Riva et al., 2016).

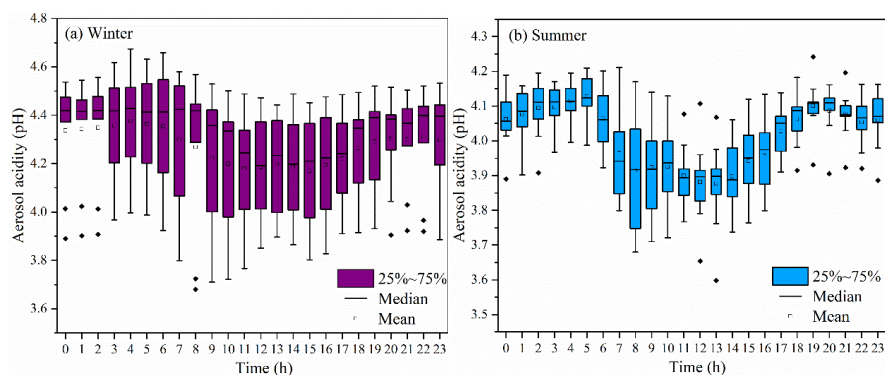
349 CPA, the typical tracer of sesquiterpenes, is formed by the photooxidation of β -
350 caryophyllene (Jaoui et al., 2007). As shown in Fig.4, CPA in winter and summer
351 accounted for 5.0% and 2.3% of the total SOA tracers, respectively. This is because
352 that the percentage of SOA_I has significant increase in summer. And the concentrations
353 of CPA ($2.5 \pm 2.0 \text{ ng m}^{-3}$) in summer were higher than that ($1.7 \pm 0.8 \text{ ng m}^{-3}$) in winter,
354 probably attributed to the emissions of β -caryophyllene driven by temperature and solar
355 radiation. The CPA has a good correlation with DHOPA in summer (Fig.S2),
356 suggesting the influence of photochemical oxidation (Liu et al., 2020). However, the
357 CPA were not correlated with LEV in both seasons, reflecting the limited contribution
358 of biomass burning (Zhang et al., 2019c).

359 *3.4 Impacts of aerosol acidity on BSOA formation*

360 Aerosol acidity (pH) was an important factor on SOA formation (Surratt et al.,
361 2007; Offenberg et al., 2009; Zhang et al., 2019b; Zhang et al., 2019d). Time series of
362 aerosol pH calculated by ISORROPIA II is shown in Fig.5. The PM_{2.5} in Xiamen was
363 moderately acidic with daily pH range from 3.68 to 4.67. The highest aerosol pH was



364 observed in winter, and the lowest pH in summer. This is with similar seasonal trend,
365 closing to the Yangtze River Delta (YRD) region, but obviously lower levels than those
366 in NCP cities of China (Zhou et al., 2021). In general, the aerosol pH in Chinese cities
367 were higher than those in US and European.



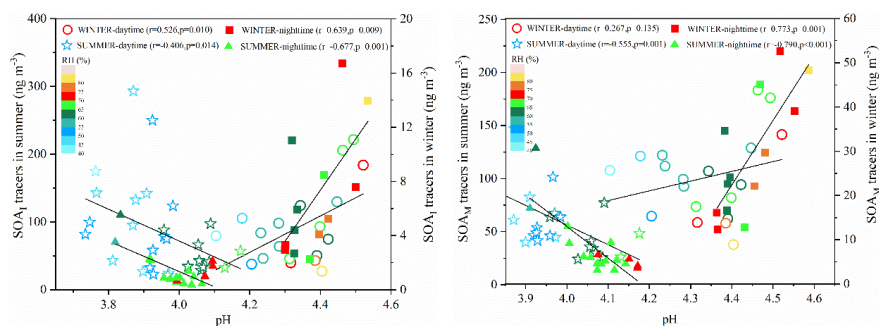
368

369 **Figure 5. Diurnal variations of aerosol acidity (pH) during the wintertime and**
370 **summertime period (The boxes with error bars represent the 10th, 25th, 75th,**
371 **and 90th percentiles)**

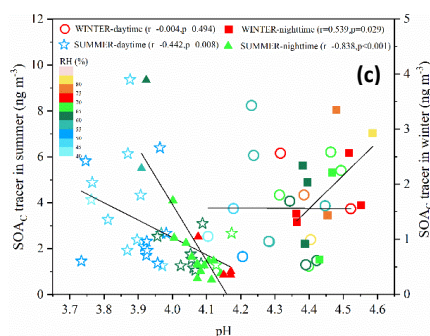
372 A declining trend pH during the daytime was observed (Fig. 5), which was related
373 to the changes of chemical compositions and environmental conditions. The aerosol pH
374 levels (~3 to 6) was related with a shift from sulfate- to nitrate-dominated aerosols (Guo
375 et al., 2017). According to the multiphase buffer theory, the peak buffer pH (pKa*)
376 regulated the aerosol pH, and temperature could obviously cause the variation of
377 aerosol pH (Zheng et al., 2020). To further discuss the impacts of aerosol acidity on
378 BSOA formation in coastal city, we analyzed the relationship between BSOA tracers
379 and seed particles with different pH and liquid water content (LWC) (Fig. 6 and Table
380 1).



381



382



383 **Figure 6. Correlations of SOA_I tracers (a), SOA_M tracers (b), SOA_C tracer (c)**
384 **with aerosol acidity (pH) during the daytime and night-time**

385 In Table 1, the BSOA tracers was linearly correlated with aerosol acidity (pH) and
386 SO₄²⁻. In summer, BSOA tracers in the particle phase were found to increase with
387 increasing acidity, which was attributed to the presence of acid catalyzed aerosols. For
388 example, isoprene SOA tracers is mainly formed through acid-catalyzed reactive
389 uptake of isoprene-derived epoxydiols (IEPOX) onto sulfate aerosol particles. In our
390 previous studies, we have reported that high concentration of MTLs was related with
391 sulfate, which could significantly promote the formation of isoprene-SOA tracers (Liu
392 et al., 2020). Other studies also found that sulfate could increase the BSOA production
393 by promoting acid-catalyzed ring-opening reactions (Xu et al., 2015). In contrast,
394 positive correlations between BSOA tracers and aerosol pH in winter were observed,
395 indicating that the formation of BSOA was predominantly enhanced by other factors,
396 except for the aerosol acidity. The aerosol pH in winter was higher than those in summer,
397 probably due to the influence of nitrate-dominated aerosols. Also, the aged aerosols



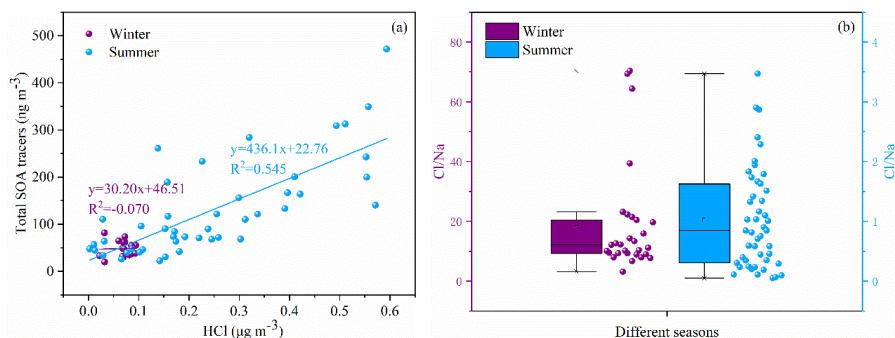
398 through long-range transport might result in the increase of BSOA tracers and aerosol
399 pH.

400 In addition, positive correlation between BSOA tracers and LWC was observed
401 (Table 1), probably attributed to the effects of the LWC on determining the peak buffer
402 pH (pK_a^*). Zheng et al. (2020) reported that the buffering effect of ammonia suppresses
403 the contribution of different chemical compositions in aerosol particles, making LWC
404 the primary determinant of aerosol pH. Other studies have demonstrated that the uptake
405 coefficient of first-generation oxidation products, especially for carbonyl compounds,
406 might depend on RH (Luo et al., 2019). Meanwhile, high LWC could reduce the aerosol
407 particle viscosity, which was benefit to the generation of the reactive intermediate such
408 as IEPOX, or other oxidation products of VOC into aqueous-phase of aerosol particles,
409 thereby promoting the formation of BSOA (Zhang et al., 2019b; Zhang et al., 2019d).

410 3.5 Impacts of chlorine on BSOA formation

411 Halogen radicals (Cl, Br and I) originated from sea salt aerosol (SSA) have an
412 important role in tropospheric oxidants chemistry (Wang et al., 2021c). In this study,
413 chlorine depletion was frequently observed in summer (Fig. 7a), indicating that HCl can
414 be formed through acid displacement of sea salt aerosol Cl^- by H_2SO_4 and HNO_3
415 produced from anthropogenic emissions of SO_2 and NO_x . Moreover, concentrations of
416 the total SOA tracers were positively correlated with HCl (Fig. 7a), suggesting the
417 enhancement of SOA precursors transformation. Previous studies have found that Cl-
418 initiated VOC oxidations could contribute to the formation of SOA (Wang and Ruiz,
419 2017; Dhulipala et al., 2019).

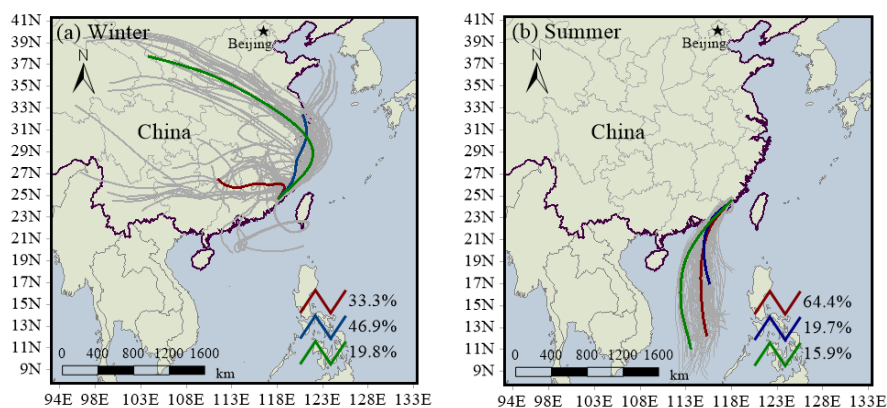
420





421 **Figure 7. Correlations of total SOA tracers and HCl (a) and chlorine depletion**
422 **(b) in different seasons**

423 Under ammonia-rich conditions, HCl partitioned into the aqueous particulate
424 phase mostly took place, and chlorine ions could affect aqueous oxidation of secondary
425 organic compounds (Xu et al., 2021). As shown in Table 1, the correlations of SOA
426 tracers in winter were found to increase with increasing NH_3 and chlorine ions in $\text{PM}_{2.5}$,
427 while inverse results were observed in summer. In winter, the dominant wind direction
428 is northeast (Fig.8), and chlorine mainly come from continental polluted air mass, such
429 as industrial and combustion emissions. So, anthropogenic pollutants through long-
430 range transport might cause the enhancement of SOA tracer concentrations at the
431 monitoring site. However, in summer, negative correlations of BSOA tracers and
432 chlorine ions in $\text{PM}_{2.5}$ was found, probably due to the influence of chlorine depletion.
433 As shown in Fig. 8, the dominant wind direction is southerly, and chlorine mainly
434 originated from the spray of sea salt.



435

436 **Figure 8. Backward trajectories analyses during the winter (a) and summertime**
437 **(b)**

438 *3.6. Enhanced formation of BSOA by anthropogenic emissions*

439 Recent studies had indicated that anthropogenic emissions might affect SOA
440 formation through multiple chemical processes, based on laboratory studies and field



441 observations (Kari et al., 2019; Shrivastava et al., 2019; Zhang et al., 2019c; Cheng et
442 al., 2021; Xu et al., 2021). In this study, we conducted the correlation analysis of
443 individual SOA tracers and $O_x(=O_3+NO_2)$, HONO, OH, SO_2 , NH_3 , $PM_{2.5}$, sulfate,
444 nitrate, as well as meteorological parameters (including T, RH and UV) (Table 1).

445 Most of SOA tracers have a significant positive correlation with NH_3 , suggesting
446 an enhancement effect on the formation of SOA (Table 1). NH_3 could affect the SOA
447 yields through both gas-phase and heterogeneous reactions (Na et al., 2007; Ma et al.,
448 2018; Hao et al., 2020). Gas-phase reaction between NH_3 and organic acids (such as
449 PA and PNA) produced ammonium salts in the particle phase, which contributed to the
450 increased SOA formation. However, not all gas-phase organic acids (e.g., MGA and
451 pyruvic acid) could demonstrate gas-to-particle conversion (Na et al., 2007). When
452 SOA formation had ceased, the addition of excessive NH_3 would result in the rapid
453 decomposition of the main SOA species, due to the nucleophilic attack of NH_3 (Ma et
454 al., 2018).

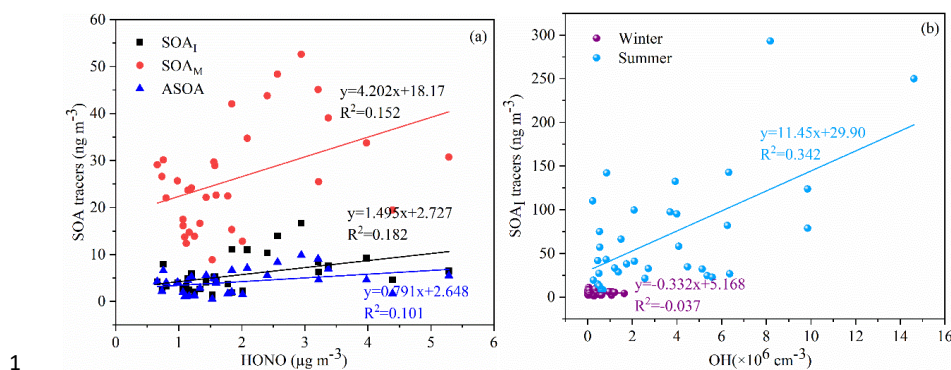
455



Table 1 Correlations between individual BSOA tracer and environmental factors in winter and summer

Season	SOA tracer	pH	LWC	HONO	PM _{2.5}	Cl ⁻	NO ₃ ⁻	SO ₄ ²⁻	NH ₃	SO ₂	NO ₂	Ox	T	RH	UV
WINTER (n=39)	C5	.584**	.701**	.534**	.690**	.569**	.710**	.663**	.705**	.308	.353*	0.203	.361*	0.140	0.200
	MTLs	.590**	.705**	.431*	.665**	.639**	.707**	.651**	.757**	0.185	0.229	0.098	.353*	0.295	-0.068
	MGA	.390*	.707**	0.261	.668**	0.081	.758**	.572**	0.284	0.172	0.123	.374*	.377*	-0.019	0.238
	PA	.432*	.403**	.463**	.407**	.481*	.416*	.488**	.440*	.446*	0.241	-0.193	.319*	-0.205	0.145
	PNA	.489**	.579**	0.311	.459**	.516**	.573**	.533**	.543**	0.08	0.071	-0.101	0.121	.337*	-0.122
	HGA	.443*	.829**	.352*	.834**	.600**	.847**	.754**	.641**	.641**	0.275	0.299	.451**	0.043	0.210
	MBTCA	.433*	.678**	.447**	.670**	.435*	.733**	.589**	.710**	.327*	0.253	.492**	.552**	-0.158	0.317
	HDMGA	.421*	.876**	.401*	.867**	.631**	.884**	.813**	.643**	.335*	0.126	.526**	.485**	-0.049	0.327
	AGA	.570**	.575**	.370*	.488**	.577**	.566**	.544**	.731**	.731**	0.126	0.181	0.019	0.279	0.298
	CPA	0.212	.462**	-0.068	.452**	.483**	.437*	.419*	.419*	0.255	-0.15	-0.170	0.016	0.079	0.200
SUMMER (n=50)	C5	-.495**	.425**	0.160	.622**	-.340*	0.268	.625**	.436**	0.254	0.025	.649**	.573**	-.529**	0.247
	MTLs	-.551**	0.131	0.055	0.272	-.439**	0.131	.428**	.304*	0.089	-0.278	.550**	.610**	-.594**	0.263
	MGA	-.540**	0.029	0.116	0.132	-.403**	0.066	.472**	0.270	0.096	-0.410**	.443**	.633**	-.668**	.382*
	PA	-.633**	.483**	.601**	.461**	-0.135	.541**	.502**	.405*	0.037	0.238	.456**	.626**	-.558**	.400*
	PNA	-.664**	.616**	.387**	.812**	-.389**	.450**	.784**	.503**	0.269	.294*	.769**	.718**	-.631**	.404*
	HGA	-.607**	.612**	.299*	.836**	-.384**	.447**	.770**	.539**	.316*	0.272	.808**	.670**	-.599**	0.322
	MBTCA	-.752**	.415**	0.237	.577**	-.382**	.359*	.636**	.501**	0.201	-0.052	.712**	.852**	-.816**	.588**
	HDMGA	-.525**	.618**	.299*	.833**	-.342*	.408**	.768**	.488**	.358*	0.244	.365**	.746**	-.500**	0.240
	AGA	-.684**	.592**	.447**	.766**	-.334*	.479**	.735**	.435**	0.244	0.271	.694**	.720**	-.634**	.477**
	CPA	-.552**	.625**	.441**	.780**	-.280*	.453**	.763**	.307*	.299*	.503**	.611**	.529**	-.458**	0.305

**Correlation coefficients with an asterisk indicate statistically significant relationships at $\alpha = 0.05$, and two asterisks mean significant at $\alpha = 0.01$.



2 **Figure 9. Relationships of SOA tracers and HONO and its estimated OH**

3 As an indicator of atmospheric oxidation capacity, the tropospheric odd oxygen
4 Ox (O₃+NO₂) was calculated. As shown in Table 1, the majority of SOA tracers in
5 summer showed significant positive correlations with Ox (R>0.5, P<0.001). However,
6 in winter, a part of SOA_M tracers (e.g. HGA, MBTCA and HDMGA) were found to be
7 significantly correlated with Ox. In addition, HONO and OH radicals, another critical
8 indicator of atmospheric oxidation capacity, was also discussed. In this study, the
9 concentration of OH radicals calculated from HONO in summer was higher than those
10 in winter. In summer, the SOA_I tracers was correlated with OH radicals (Fig.9b),
11 consisted with previous findings that OH radicals could promote the formation of SOA
12 (Sarrafzadeh et al., 2016; Liu et al., 2019; Song et al., 2019; Zhang et al., 2019a). Due
13 to its photolysis to produce OH radicals during the daytime, HONO could facilitate
14 SOA formation. In winter, the concentrations of SOA_I, SOA_M and ASOA tracers were
15 correlated with HONO (Fig.9a). These results indicated high concentrations of HONO
16 and sufficient ultraviolet radiation could enhance the photochemical reactions of VOCs.
17 Which was consisted with our previous results on the formation of peroxyacetyl nitrate
18 (PAN) (Hu et al., 2020). As for T and UV, it exhibited significantly positive correlations
19 with the related SOA tracers, especially in summer. These results suggested that SOA
20 tracers were produced from the photo-oxidation of VOC precursors (Cheng et al., 2021).

21 In addition, the SOA tracers were significantly positive correlated with PM_{2.5} and
22 its components including NO₃⁻ and SO₄²⁻. In coastal cities of southeastern China, with



23 the development of rapid urbanization, air pollution caused by motor vehicles and
24 industrial emissions is becoming more and more obvious in winter (Wu et al., 2020).
25 Secondary formation of PM_{2.5} accounted for 60-70% of the total fine particle, and NO₃⁻,
26 SO₄²⁻ and NH₄⁺ are significant components of secondary inorganic aerosols (Wu et al.,
27 2019; Hong et al., 2021). These results also proved the obvious effects of anthropogenic
28 emissions on secondary formation of aerosol particles under atmospheric relatively
29 stability conditions during the winter.

30 **Conclusions**

31 Pollution characteristics and source identification of BSOA tracers during the
32 summer and winter in coastal areas of southeastern China were investigated. The
33 average concentration of total BSOA tracers in summer was higher than that in winter,
34 with the predominance of SOA_M, followed by SOA_I and SOA_C. The BSOA tracers in
35 summer were predominantly produced by the influence of photochemical oxidation
36 under relatively clean conditions. However, in winter, the formation of BSOA tracers
37 were attributed to the impacts of anthropogenic emissions, reflecting the
38 anthropogenic–biogenic interactions. In addition, the results also indicated that acid-
39 catalyzed reactive uptake onto sulfate aerosol particles enhanced the formation of
40 BSOA in both seasons. We further found that Cl-initiated VOC oxidations has
41 potentially accelerated the transformation of BSOA precursors through sea salt aerosol
42 originated from the ocean in summer and anthropogenic emissions in winter. This study
43 demonstrated that the combined effects of anthropogenic pollutants and atmospheric
44 oxidation capacity on the formation of BSOA in coastal area.

45

46 **Data Availability.** The data set related to this work can be accessed via
47 <https://doi.org/10.5281/zenodo.6376025> (Hong, 2022). The details are also available
48 upon request from the corresponding author (ywhong@iue.ac.cn).

49

50

51



52

53 **Authorship Contribution Statement.** Youwei Hong and Xinbei Xu contributed equally
54 to this work. Youwei Hong designed and wrote the manuscript. Xinbei Xu collected the
55 data, contributed to the data analysis. Dan Liao, Taotao Liu, Xiaoting Ji and Ke Xu
56 performed modeling analyses and data analysis. Jinsheng Chen supported funding of
57 observation and research. Chunyang Liao, Ting Wang and Chunshui Lin contributed to
58 revise the manuscript.

59

60 **Competing interests.** The authors declare that they have no conflict of interest.

61

62 **Acknowledgement.** The authors gratefully acknowledge Yanting Chen, Han Zhang and
63 Xu Liao (Institute of Urban Environment, Chinese Academy of Sciences) for the
64 guidance and assistance during sample pretreatment, and Lingling Xu and Mengren Li
65 (Institute of Urban Environment, Chinese Academy of Sciences) for the discussion of
66 this paper.

67

68 **Financial support.** This research was financially supported by the Xiamen Youth
69 Innovation Fund Project (3502Z20206094), the foreign cooperation project of Fujian
70 Province (2020I0038), the Cultivating Project of Strategic Priority Research Program
71 of Chinese Academy of Sciences (XDPB1903), the National Key Research and
72 Development Program (2016YFC0112200), State Key Laboratory of Environmental
73 Chemistry and Ecotoxicology, Research Center for Eco-Environmental Sciences, CAS
74 (KF2020-06), the FJIRSM&IUE Joint Research Fund (RHZX-2019-006) and center for
75 Excellence in Regional Atmospheric Environment project (EOL1B20201).

76

77

78

79

80

81



82 Reference

- 83 Charan, S.M., Huang, Y., Seinfeld, J.H., 2019. Computational Simulation of Secondary
84 Organic Aerosol Formation in Laboratory Chambers. *Chem. Rev.* 119, 11912-11944.
- 85 Cheng, Y., Ma, Y., Hu, D., 2021. Tracer-based source apportioning of atmospheric organic
86 carbon and the influence of anthropogenic emissions on secondary organic aerosol
87 formation in Hong Kong. *Atmos. Chem. Phys.* 21, 10589-10608.
- 88 Dhulipala, S.V., Bhandari, S., Hildebrandt Ruiz, L., 2019. Formation of oxidized organic
89 compounds from Cl-initiated oxidation of toluene. *Atmospheric Environment* 199, 265-
90 273.
- 91 Ding, X., He, Q.-F., Shen, R.-Q., Yu, Q.-Q., Wang, X.-M., 2014. Spatial distributions of
92 secondary organic aerosols from isoprene, monoterpenes, beta-caryophyllene, and
93 aromatics over China during summer. *Journal of Geophysical Research-Atmospheres*
94 119, 11877-11891.
- 95 Friese, E., Ebel, A., 2010. Temperature Dependent Thermodynamic Model of the System
96 $H^+ - NH_4^+ - Na^+ - SO_4^{2-} - NO_3^- - Cl^- - H_2O$. *The Journal of Physical Chemistry A* 114,
97 11595-11631.
- 98 Fu, P., Kawamura, K., Chen, J., Barrie, L.A., 2009. Isoprene, Monoterpene, and
99 Sesquiterpene Oxidation Products in the High Arctic Aerosols during Late Winter to
100 Early Summer. *Environmental Science & Technology* 43, 4022-4028.
- 101 Guo, H., Weber, R.J., Nenes, A., 2017. High levels of ammonia do not raise fine particle pH
102 sufficiently to yield nitrogen oxide-dominated sulfate production. *Scientific Reports* 7,
103 12109.
- 104 Hallquist, M., Wenger, J.C., Baltensperger, U., Rudich, Y., Simpson, D., Claeys, M.,
105 Dommen, J., Donahue, N.M., George, C., Goldstein, A.H., Hamilton, J.F., Herrmann, H.,
106 Hoffmann, T., Iinuma, Y., Jang, M., Jenkin, M.E., Jimenez, J.L., Kiendler-Scharr, A.,
107 Maenhaut, W., McFiggans, G., Mentel, T.F., Monod, A., Prevot, A.S.H., Seinfeld, J.H.,
108 Surratt, J.D., Szmigielski, R., Wildt, J., 2009. The formation, properties and impact of
109 secondary organic aerosol: current and emerging issues. *Atmospheric Chemistry and*
110 *Physics* 9, 5155-5236.
- 111 Hao, L., Kari, E., Leskinen, A., Worsnop, D.R., Virtanen, A., 2020. Direct contribution of
112 ammonia to α -pinene secondary organic aerosol formation. *Atmos. Chem. Phys.* 20,
113 14393-14405.
- 114 Hong, Y., Xu, X., Liao, D., Zheng, R., Ji, X., Chen, Y., Xu, L., Li, M., Wang, H., Xiao, H.,
115 Choi, S.-D., Chen, J., 2021. Source apportionment of PM_{2.5} and sulfate formation



- 116 during the COVID-19 lockdown in a coastal city of southeast China. *Environmental*
117 *Pollution* 286, 117577.
- 118 Hong, Z., Zhang, H., Zhang, Y., Xu, L., Liu, T., Xiao, H., Hong, Y., Chen, J., Li, M., Deng,
119 J., Wu, X., Hu, B., Chen, X., 2019. Secondary organic aerosol of PM_{2.5} in a
120 mountainous forest area in southeastern China: Molecular compositions and tracers
121 implication. *Science of the Total Environment* 653, 496-503.
- 122 Hoyle, C.R., Boy, M., Donahue, N.M., Fry, J.L., Glasius, M., Guenther, A., Hallar, A.G.,
123 Hartz, K.H., Petters, M.D., Petaja, T., Rosenoern, T., Sullivan, A.P., 2011. A review of
124 the anthropogenic influence on biogenic secondary organic aerosol. *Atmospheric*
125 *Chemistry and Physics* 11, 321-343.
- 126 Hu, B., Liu, T., Hong, Y., Xu, L., Li, M., Wu, X., Wang, H., Chen, J., Chen, J., 2020.
127 Characteristics of peroxyacetyl nitrate (PAN) in a coastal city of southeastern China:
128 Photochemical mechanism and pollution process. *Science of the Total Environment* 719.
- 129 Jaoui, M., Kleindienst, T.E., Lewandowski, M., Offenberg, J.H., Edney, E.O., 2005.
130 Identification and quantification of aerosol polar oxygenated compounds bearing
131 carboxylic or hydroxyl groups. 2. Organic tracer compounds from monoterpenes.
132 *Environmental Science & Technology* 39, 5661-5673.
- 133 Jaoui, M., Lewandowski, M., Kleindienst, T.E., Offenberg, J.H., Edney, E.O., 2007. β -
134 caryophyllinic acid: An atmospheric tracer for β -caryophyllene secondary organic
135 aerosol. *Geophysical Research Letters* 34.
- 136 Kari, E., Hao, L.Q., Ylisirnio, A., Buchholz, A., Leskinen, A., Yli-Pirila, P., Nuutinen, I.,
137 Kuuspallo, K., Jokiniemi, J., Faiola, C.L., Schobesberger, S., Virtanen, A., 2019.
138 Potential dual effect of anthropogenic emissions on the formation of biogenic secondary
139 organic aerosol (BSOA). *Atmospheric Chemistry and Physics* 19, 15651-15671.
- 140 Kleindienst, T.E., Jaoui, M., Lewandowski, M., Offenberg, J.H., Lewis, C.W., Bhawe, P.V.,
141 Edney, E.O., 2007. Estimates of the contributions of biogenic and anthropogenic
142 hydrocarbons to secondary organic aerosol at a southeastern US location. *Atmospheric*
143 *Environment* 41, 8288-8300.
- 144 Lewandowski, M., Piletic, I.R., Kleindienst, T.E., Offenberg, J.H., Beaver, M.R., Jaoui, M.,
145 Docherty, K.S., Edney, E.O., 2013. Secondary organic aerosol characterisation at field
146 sites across the United States during the spring-summer period. *International Journal of*
147 *Environmental Analytical Chemistry* 93, 1084-1103.
- 148 Liu, S., Huang, D., Wang, Y., Zhang, S., Wu, C., Du, W., Wang, G., 2021. Synergetic effect
149 of NH₃ and NO_x on the production and optical absorption of secondary organic aerosol
150 formation from toluene photooxidation. *Atmos. Chem. Phys.* 21, 17759–17773.



- 151 Liu, S., Tsona, N.T., Zhang, Q., Jia, L., Xu, Y., Du, L., 2019. Influence of relative humidity
152 on cyclohexene SOA formation from OH photooxidation. *Chemosphere* 231, 478-486.
- 153 Liu, T., Hu, B., Xu, X., Hong, Y., Zhang, Y., Wu, X., Xu, L., Li, M., Chen, Y., Chen, X.,
154 Chen, J., 2020. Characteristics of PM_{2.5}-bound secondary organic aerosol tracers in a
155 coastal city in Southeastern China: Seasonal patterns and pollution identification.
156 *Atmospheric Environment* 237.
- 157 Luo, H., Jia, L., Wan, Q., An, T., Wang, Y., 2019. Role of liquid water in the formation of O-
158 3 and SOA particles from 1,2,3-trimethylbenzene. *Atmospheric Environment* 217.
- 159 Lv, S., Wang, F., Wu, C., Chen, Y., Liu, S., Zhang, S., Li, D., Du, W., Zhang, F., Wang, H.,
160 Huang, C., Fu, Q., Duan, Y., Wang, G., 2022. Gas-to-Aerosol Phase Partitioning of
161 Atmospheric Water-Soluble Organic Compounds at a Rural Site in China: An Enhancing
162 Effect of NH₃ on SOA Formation. *Environmental Science & Technology*.
- 163 Ma, Q., Lin, X.X., Yang, C.G., Long, B., Gai, Y.B., Zhang, W.J., 2018. The influences of
164 ammonia on aerosol formation in the ozonolysis of styrene: roles of Criegee intermediate
165 reactions. *Roy Soc Open Sci* 5.
- 166 Mahilang, M., Deb, M.K., Pervez, S., 2021. Biogenic secondary organic aerosols: A review
167 on formation mechanism, analytical challenges and environmental impacts.
168 *Chemosphere* 262.
- 169 McFiggans, G., Mentel, T.F., Wildt, J., Pullinen, I., Kang, S., Kleist, E., Schmitt, S., Springer,
170 M., Tillmann, R., Wu, C., Zhao, D.F., Hallquist, M., Faxon, C., Le Breton, M., Hallquist,
171 A.M., Simpson, D., Bergstrom, R., Jenkin, M.E., Ehn, M., Thornton, J.A., Alfarra, M.R.,
172 Bannan, T.J., Percival, C.J., Priestley, M., Topping, D., Kiendler-Scharr, A., 2019.
173 Secondary organic aerosol reduced by mixture of atmospheric vapours. *Nature* 565, 587-
174 593.
- 175 Na, K., Song, C., Switzer, C., Cocker, D.R., 2007. Effect of Ammonia on Secondary Organic
176 Aerosol Formation from α -Pinene Ozonolysis in Dry and Humid Conditions.
177 *Environmental Science & Technology* 41, 6096-6102.
- 178 Newland, M.J., Bryant, D.J., Dunmore, R.E., Bannan, T.J., Acton, W.J.F., Langford, B.,
179 Hopkins, J.R., Squires, F.A., Dixon, W., Drysdale, W.S., Ivatt, P.D., Evans, M.J.,
180 Edwards, P.M., Whalley, L.K., Heard, D.E., Slater, E.J., Woodward-Massey, R., Ye, C.,
181 Mehra, A., Worrall, S.D., Bacak, A., Coe, H., Percival, C.J., Hewitt, C.N., Lee, J.D., Cui,
182 T., Surratt, J.D., Wang, X., Lewis, A.C., Rickard, A.R., Hamilton, J.F., 2021. Low-NO
183 atmospheric oxidation pathways in a polluted megacity. *Atmos. Chem. Phys.* 21, 1613-
184 1625.



- 185 Offenberg, J.H., Lewandowski, M., Edney, E.O., Kleindienst, T.E., Jaoui, M., 2009. Influence
186 of Aerosol Acidity on the Formation of Secondary Organic Aerosol from Biogenic
187 Precursor Hydrocarbons. *Environmental Science & Technology* 43, 7742-7747.
- 188 Offenberg, J.H., Lewis, C.W., Lewandowski, M., Jaoui, M., Kleindienst, T.E., Edney, E.O.,
189 2007. Contributions of toluene and alpha-pinene to SOA formed in an irradiated
190 toluene/alpha-pinene/NO_x/air mixture: Comparison of results using C-14 content and
191 SOA organic tracer methods. *Environmental Science & Technology* 41, 3972-3976.
- 192 Palmer, P.I., Marvin, M.R., Siddans, R., Kerridge, B.J., Moore, D.P., 2022. Nocturnal
193 survival of isoprene linked to formation of upper tropospheric organic aerosol. *Science*
194 375, 562-566.
- 195 Reid, J.P., Bertram, A.K., Topping, D.O., Laskin, A., Martin, S.T., Petters, M.D., Pope, F.D.,
196 Rovelli, G., 2018. The viscosity of atmospherically relevant organic particles. *Nature*
197 *Communications* 9.
- 198 Riva, M., Budisulistiorini, S.H., Zhang, Z., Gold, A., Surratt, J.D., 2016. Chemical
199 characterization of secondary organic aerosol constituents from isoprene ozonolysis in
200 the presence of acidic aerosol. *Atmospheric Environment* 130, 5-13.
- 201 Sarrafzadeh, M., Wildt, J., Pullinen, I., Springer, M., Kleist, E., Tillmann, R., Schmitt, S.H.,
202 Wu, C., Mentel, T.F., Zhao, D., Hastie, D.R., Kiendler-Scharr, A., 2016. Impact of NO_x
203 and OH on secondary organic aerosol formation from beta-pinene photooxidation.
204 *Atmospheric Chemistry and Physics* 16, 11237-11248.
- 205 Shrivastava, M., Andreae, M.O., Artaxo, P., Barbosa, H.M.J., Berg, L.K., Brito, J., Ching, J.,
206 Easter, R.C., Fan, J., Fast, J.D., Feng, Z., Fuentes, J.D., Glasius, M., Goldstein, A.H.,
207 Alves, E.G., Gomes, H., Gu, D., Guenther, A., Jathar, S.H., Kim, S., Liu, Y., Lou, S.,
208 Martin, S.T., McNeill, V.F., Medeiros, A., de Sa, S.S., Shilling, J.E., Springston, S.R.,
209 Souza, R.A.F., Thornton, J.A., Isaacman-VanWertz, G., Yee, L.D., Ynoue, R., Zaveri,
210 R.A., Zelenyuk, A., Zhao, C., 2019. Urban pollution greatly enhances formation of
211 natural aerosols over the Amazon rainforest. *Nature Communications* 10.
- 212 Shrivastava, M., Cappa, C.D., Fan, J., Goldstein, A.H., Guenther, A.B., Jimenez, J.L., Kuang,
213 C., Laskin, A., Martin, S.T., Ng, N.L., Petaja, T., Pierce, J.R., Rasch, P.J., Roldin, P.,
214 Seinfeld, J.H., Shilling, J., Smith, J.N., Thornton, J.A., Volkamer, R., Wang, J.,
215 Worsnop, D.R., Zaveri, R.A., Zelenyuk, A., Zhang, Q., 2017. Recent advances in
216 understanding secondary organic aerosol: Implications for global climate forcing.
217 *Reviews of Geophysics* 55, 509-559.
- 218 Song, M., Zhang, C., Wu, H., Mu, Y., Ma, Z., Zhang, Y., Liu, J., Li, X., 2019. The influence
219 of OH concentration on SOA formation from isoprene photooxidation. *Science of the*
220 *Total Environment* 650, 951-957.



- 221 Surratt, J.D., Chan, A.W.H., Eddingsaas, N.C., Chan, M., Loza, C.L., Kwan, A.J., Hersey,
222 S.P., Flagan, R.C., Wennberg, P.O., Seinfeld, J.H., 2010. Reactive intermediates
223 revealed in secondary organic aerosol formation from isoprene. *Proceedings of the*
224 *National Academy of Sciences of the United States of America* 107, 6640-6645.
- 225 Surratt, J.D., Lewandowski, M., Offenberg, J.H., Jaoui, M., Kleindienst, T.E., Edney, E.O.,
226 Seinfeld, J.H., 2007. Effect of acidity on secondary organic aerosol formation from
227 isoprene. *Environmental Science & Technology* 41, 5363-5369.
- 228 Wang, D.S., Ruiz, L.H., 2017. Secondary organic aerosol from chlorine-initiated oxidation of
229 isoprene. *Atmos. Chem. Phys.* 17, 13491-13508.
- 230 Wang, J., Ye, J., Zhang, Q., Zhao, J., Wu, Y., Li, J., Liu, D., Li, W., Zhang, Y., Wu, C., Xie,
231 C., Qin, Y., Lei, Y., Huang, X., Guo, J., Liu, P., Fu, P., Li, Y., Lee, H.C., Choi, H.,
232 Zhang, J., Liao, H., Chen, M., Sun, Y., Ge, X., Martin, S.T., Jacob, D.J., 2021a. Aqueous
233 production of secondary organic aerosol from fossil-fuel emissions in winter Beijing
234 haze. *Proceedings of the National Academy of Sciences of the United States of America*
235 118.
- 236 Wang, J., Ye, J., Zhang, Q., Zhao, J., Wu, Y., Li, J., Liu, D., Li, W., Zhang, Y., Wu, C., Xie,
237 C., Qin, Y., Lei, Y., Huang, X., Guo, J., Liu, P., Fu, P., Li, Y., Lee, H.C., Choi, H.,
238 Zhang, J., Liao, H., Chen, M., Sun, Y., Ge, X., Martin, S.T., Jacob, D.J., 2021b. Aqueous
239 production of secondary organic aerosol from fossil-fuel emissions in winter Beijing
240 haze. *Proc Natl Acad Sci U S A* 118.
- 241 Wang, S., Du, L., Tsona, N.T., Jiang, X., You, B., Xu, L., Yang, Z., Wang, W., 2020. Effect
242 of NO_x and SO₂ on the photooxidation of methylglyoxal: Implications in secondary
243 aerosol formation. *J Environ Sci (China)* 92, 151-162.
- 244 Wang, X., Jacob, D.J., Downs, W., Zhai, S., Zhu, L., Shah, V., Holmes, C.D., Sherwen, T.,
245 Alexander, B., Evans, M.J., Eastham, S.D., Neuman, J.A., Veres, P.R., Koenig, T.K.,
246 Volkamer, R., Huey, L.G., Bannan, T.J., Percival, C.J., Lee, B.H., Thornton, J.A., 2021c.
247 Global tropospheric halogen (Cl, Br, I) chemistry and its impact on oxidants. *Atmos.*
248 *Chem. Phys.* 21, 13973-13996.
- 249 Wen, L., Chen, T., Zheng, P., Wu, L., Wang, X., Mellouki, A., Xue, L., Wang, W., 2019.
250 Nitrous acid in marine boundary layer over eastern Bohai Sea, China: Characteristics,
251 sources, and implications. *Sci. Total Environ.*
- 252 Wu, X., Li, M., Chen, J., Wang, H., Xu, L., Hong, Y., Zhao, G., Hu, B., Zhang, Y., Dan, Y.,
253 Yu, S., 2020. The characteristics of air pollution induced by the quasi-stationary front:
254 Formation processes and influencing factors. *Science of the Total Environment* 707.
- 255 Wu, X., Xu, L.L., Hong, Y.W., Chen, J.F., Qiu, Y.Q., Hu, B.Y., Hong, Z.Y., Zhang, Y.R.,
256 Liu, T.T., Chen, Y.T., Bian, Y.H., Zhao, G.Q., Chen, J.S., Li, M.R., 2019. The air



- 257 pollution governed by subtropical high in a coastal city in Southeast China: Formation
258 processes and influencing mechanisms. *Science of the Total Environment* 692, 1135-
259 1145.
- 260 Xiao, Y., Wu, Z., Guo, S., He, L., Huang, X., Hu, M., 2020. Formation mechanism of
261 secondary organic aerosol in aerosol liquid water: A review. *Chinese Science Bulletin* 65,
262 3118-3133.
- 263 Xu, L., Du, L., Tsona, N.T., Ge, M.F., 2021. Anthropogenic Effects on Biogenic Secondary
264 Organic Aerosol Formation. *Advances in Atmospheric Sciences* 38, 1053-1084.
- 265 Xu, L., Guo, H., Boyd, C.M., Klein, M., Bougiatioti, A., Cerully, K.M., Hite, J.R., Isaacman-
266 VanWertz, G., Kreisberg, N.M., Knote, C., Olson, K., Koss, A., Goldstein, A.H., Hering,
267 S.V., de Gouw, J., Baumann, K., Lee, S.H., Nenes, A., Weber, R.J., Ng, N.L., 2015.
268 Effects of anthropogenic emissions on aerosol formation from isoprene and
269 monoterpenes in the southeastern United States. *Proc Natl Acad Sci U S A* 112, 37-42.
- 270 Yang, W., Cao, J., Wu, Y., Kong, F., Li, L., 2021. Review on plant terpenoid emissions
271 worldwide and in China. *Science of the total environment* 787, 147454-147454.
- 272 Zhang, J., An, J., Qu, Y., Liu, X., Chen, Y., 2019a. Impacts of potential HONO sources on the
273 concentrations of oxidants and secondary organic aerosols in the Beijing-Tianjin-Hebei
274 region of China. *Science of the Total Environment* 647, 836-852.
- 275 Zhang, P., Chen, T., Liu, J., Liu, C., Ma, J., Ma, Q., Chu, B., He, H., 2019b. Impacts of SO₂,
276 Relative Humidity, and Seed Acidity on Secondary Organic Aerosol Formation in the
277 Ozonolysis of Butyl Vinyl Ether. *Environmental Science & Technology* 53, 8845-8853.
- 278 Zhang, Y.-Q., Chen, D.-H., Ding, X., Li, J., Zhang, T., Wang, J.-Q., Cheng, Q., Jiang, H.,
279 Song, W., Ou, Y.-B., Ye, P.-L., Zhang, G., Wang, X.-M., 2019c. Impact of
280 anthropogenic emissions on biogenic secondary organic aerosol: observation in the Pearl
281 River Delta, southern China. *Atmospheric Chemistry and Physics* 19, 14403-14415.
- 282 Zhang, Y., Chen, Y., Lei, Z., Olson, N.E., Riva, M., Koss, A.R., Zhang, Z., Gold, A., Jayne,
283 J.T., Worsnop, D.R., Onasch, T.B., Kroll, J.H., Turpin, B.J., Ault, A.P., Surratt, J.D.,
284 2019d. Joint Impacts of Acidity and Viscosity on the Formation of Secondary Organic
285 Aerosol from Isoprene Epoxydiols (IEPDX) in Phase Separated Particles. *Acs Earth and*
286 *Space Chemistry* 3, 2646-2658.
- 287 Zhao, D.F., Schmitt, S.H., Wang, M.J., Acir, I.H., Tillmann, R., Tan, Z.F., Novelli, A., Fuchs,
288 H., Pullinen, I., Wegener, R., Rohrer, F., Wildt, J., Kiendler-Scharr, A., Wahner, A.,
289 Mentel, T.F., 2018. Effects of NO_x and SO₂ on the secondary organic aerosol formation
290 from photooxidation of alpha-pinene and limonene. *Atmospheric Chemistry and Physics*
291 18, 1611-1628.



- 292 Zheng, G., Su, H., Wang, S., Andreae, M.O., Poschl, U., Cheng, Y., 2020. Multiphase buffer
293 theory explains contrasts in atmospheric aerosol acidity. *Science* 369, 1374-+.
- 294 Zhou, M., Zheng, G., Wang, H., Qiao, L., Zhu, S., Huang, D., An, J., Lou, S., Tao, S., Wang,
295 Q., Yan, R., Ma, Y., Chen, C., Cheng, Y., Su, H., Huang, C., 2021. Long-term trends and
296 drivers of aerosol pH in eastern China. *Atmos. Chem. Phys. Discuss.* 2021, 1-21.
- 297 Zhu, J., Penner, J.E., Yu, F., Sillman, S., Andreae, M.O., Coe, H., 2019. Decrease in radiative
298 forcing by organic aerosol nucleation, climate, and land use change. *Nature*
299 *Communications* 10.

300

301

302